

Accelerated materials property predictions and design using motif-based fingerprints

Tran Doan Huan, Arun Mannodi-Kanakkithodi, and Rampi Ramprasad*

Institute of Materials Science, University of Connecticut, 97 North Eagleville Road, Unit 3136, Storrs, Connecticut 06269-3136, USA

(Received 26 March 2015; published 8 July 2015)

Data-driven approaches are particularly useful for computational materials discovery and design as they can be used for rapidly screening over a very large number of materials, thus suggesting lead candidates for further in-depth investigations. A central challenge of such approaches is to develop a numerical representation, often referred to as a fingerprint, of the materials. Inspired by recent developments in cheminformatics, we propose a class of hierarchical motif-based topological fingerprints for materials composed of elements such as C, O, H, N, F, etc., whose coordination preferences are well understood. We show that these fingerprints, when representing either molecules or crystals, may be effectively mapped onto a variety of properties using a similarity-based learning model and hence can be used to predict the relevant properties of a material, given that its fingerprint can be defined. Two simple machine-learning-based procedures are introduced to demonstrate that the learning model can be inverted to identify the desired fingerprints and then to reconstruct molecules which possess a set of targeted properties.

DOI: [10.1103/PhysRevB.92.014106](https://doi.org/10.1103/PhysRevB.92.014106)

PACS number(s): 71.15.Mb, 81.05.-t, 71.15.Dx

I. INTRODUCTION

Data-driven approaches towards materials design and discovery are rapidly increasing in popularity, demand, and potency [1–15]. This emerging trend is fueled by the availability and emergence of large materials databases [16–18], as well as our ability to progressively accumulate materials data via high-throughput computations [19,20] and experiments [16–18]. Data-driven strategies aimed at rapid property predictions and ultimately at rational or informed materials design rely on exploiting the information content of past data and using such information within heuristic or statistical interpolative learning models to provide estimates of properties of a new material. This approach is entirely analogous to similar pursuits undertaken within chem- and bioinformatics wherein lead candidates worthy of further in-depth investigations are identified rapidly in a first level of screening [4,5,14].

Data-driven property-prediction strategies have two steps. The first involves representing materials numerically via descriptors, attribute vectors, or fingerprints. In the second step, using available “training” data sets, a mapping is established between the numerical representation of materials and their properties, thus leading to a prediction model. Subsequently, the properties of a new material are estimated using this model after reducing the material to its numerical representation.

One of the central challenges in this whole process is deciding an appropriate and acceptable numerical representation of materials. The specific choice of this representation is entirely application dependent and can range from high-level descriptors (e.g., d -band center, atomic electronegativities) [21,22] to topological features (e.g., substructural motifs) [20,23,24] to microscopic fingerprints that may capture chemical and configurational degrees of freedom (e.g., Coulomb matrix, symmetry functions) [25–28]. Regardless of the specific choice, the representations are expected to satisfy certain basic requirements. These include invariance of the representation with respect to transformations of the material such as translation,

rotation, and permutation of like elements. Moreover, it is desired that the representation be intuitive, elegant, and physically and chemically meaningful.

In this contribution, inspired by developments in cheminformatics [14,15], we propose a class of hierarchical motif-based topological fingerprints (Fig. 1). This choice, in which the motifs are molecular fragments of varying sizes, is particularly suited to representing molecules and solids composed of elements such as H, C, N, O, F, etc., whose coordination preferences are well understood. Large data sets of molecules and solids are considered, and it is shown that the fingerprints may be effectively mapped to a variety of properties using a similarity-based learning algorithm. Moreover, it is demonstrated that the learning model may be inverted to identify fingerprints and, subsequently, to reconstruct actual molecules that possess a desired set of target properties.

II. DATA SETS

In the present work, we restrict ourselves to systems composed of C, O, and H. We used two data sets, one for molecules and one for crystals, to demonstrate the applicability of the proposed fingerprints. Of these two data sets, the former was taken from Ref. [19], while the latter was prepared by us.

A. Molecule data set

A data set of more than 134 000 small molecules made up of C, O, H, N, and F was reported in Ref. [19]. This reliable data set, which contains the optimized geometries and energetic, electronic, and thermodynamic properties calculated using the Becke, three-parameter, Lee-Yang-Parr (B3LYP) hybrid exchange-correlation (XC) functional and the split-valence basis set of 6-31G(2d,p) type basis set with the GAUSSIAN 09 software, sets the stage for many interesting data-mining works [29,30]. A subset of this data set, containing 45 708 molecules composed of C, O, and H, was used in this work. Five properties were considered, including the atomization energy \mathcal{E}_{at} , the energy gap E_{HL} between the highest occupied and lowest unoccupied molecular orbitals (HOMO-LUMO gap), the isotropic

*rampi.ramprasad@uconn.edu

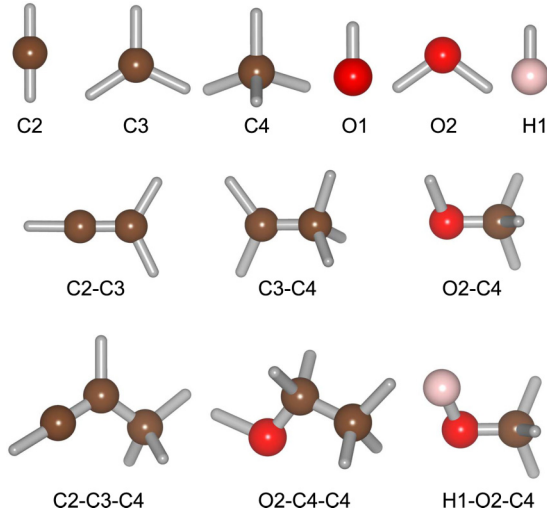


FIG. 1. (Color online) Illustration of motifs of several types, including the atom types ($\mathcal{A}i$, top row), some of the bond types ($\mathcal{A}i-Bj$, middle row), and two-bond catenations ($\mathcal{A}i-Bj-Ck$, bottom row) of materials composed by carbon, oxygen, and hydrogen.

polarizability α , the heat capacity C_v , and the zero-point vibration energy \mathcal{E}_{zp} .

B. Crystal data set

In addition to the molecule data set, we prepared another data set of 215 organic crystals comprising C, O, and H. This includes (1) 12 existing polymers composed of C, O, and H, (2) 16 new polymer structures predicted by the minima-hopping method [31–33] and USPEX [34] for 16 quasi-one-dimensional polymer chain models reported in Ref. [3], and (3) 34 organic crystals composed of C and H and 153 organic crystals composed of C, O, and H obtained from the Crystallography Open Database [18].

The obtained structures were optimized by first-principles calculations within the density functional theory (DFT) formalism as implemented in the Vienna Ab initio Simulation Package (VASP) [35–38], utilizing the semilocal refitted Perdew-Wang 86 (rPW86) XC functional [39] and a plane-wave energy cutoff of 400 eV. A Monkhorst-Pack \mathbf{k} -point mesh [40] with a spacing of no more than 0.15 \AA^{-1} in the reciprocal space were used for sampling the Brillouin zone, while the van der Waals interactions were estimated with the nonlocal density functional vdW-DF2 [41]. Convergence was assumed when the atomic forces exerting on the atomic sites were smaller than 0.01 eV/\AA . The entire crystal data set, which includes the optimized structures, the atomization energies \mathcal{E}_{at} , the band gaps E_g , and the electronic and ionic parts of the dielectric constants, ϵ_{elec} and ϵ_{ion} , can be found in the Supplemental Material [42].

III. FINGERPRINTS

A hierarchy of equilibrium structure fingerprints of the same family with increasing levels of sophistication is proposed here. The construction of fingerprints was guided by two simple chemical concepts, i.e., **chemical bonds** and **coordination number**. The former intuitively characterizes the

short-range interatomic interactions [43], while the latter is the number of bonds involving a given atom. In major classes of materials composed of light elements such as C, H, O, N, and F, these concepts are well defined. In particular, the length of a given bond involving these elements falls in a narrow range (see Refs. [44,45] for a comprehensive bond length statistics). For instance, the equilibrium length of a single bond between two C atoms is $\simeq 1.50 \text{ \AA}$, the length of a double bond between two C atoms is $\simeq 1.45 \text{ \AA}$, and the length of a double bond between a C atom and an O atom is $\simeq 1.20 \text{ \AA}$ [44,45]. The coordination number is also well defined; that is, for a C atom, it can be only 2, 3, or 4, while each O atom can generally bond with 1 or 2 other atoms. **Therefore, atoms in a structure can be unambiguously classified (or labeled) by $\mathcal{A}i$, where \mathcal{A} is the type of the element ($\mathcal{A} \in \{\text{C, O, H}\}$) and i is its coordination number. Likewise, bonds can be specified by the types of its two ends, e.g., $\mathcal{A}i-Bj$.** For the data sets of C, O, and H, the six possible atom types are C2, C3, C4, O1, O2, and H1, while there are 16 chemically permissible types of bonds, namely, C2–C2, C2–C3, C2–C4, C2–O1, C2–O2, C2–H1, C3–C3, C3–C4, C3–O1, C3–O2, C3–H1, C4–C4, C4–O2, C4–H1, O2–O2, and O2–H1. Except for C2–O1, C2–O2, and O2–O2, 13 of them are present in our molecule and crystal data sets. The atom and bond types belong to a family of related structural building units (Fig. 1, subsequently described) that can be used to numerically represent the materials structures and hence are used to define the fingerprints. In particular, the i th-order fingerprint $\mathbf{f}^{(i)}$ is defined in terms of its components as

$$f_{\kappa}^{(i)} = \frac{n_{\kappa}^{(i)}}{N_{at}}. \quad (1)$$

Here, $n_{\kappa}^{(i)}$ is the number of building units (or fragments or motifs) of type κ , and N_{at} is the number of atoms either in the molecule or in the unit cell of a crystal. Four types of fingerprints, namely, $\mathbf{f}^{(0)}$, $\mathbf{f}^{(1)}$, $\mathbf{f}^{(2)}$, and $\mathbf{f}^{(3)}$, are discussed in the following sections.

A. Zeroth-order fingerprint $\mathbf{f}^{(0)}$

The simplest (zeroth-order) fingerprint $\mathbf{f}^{(0)}$ represents the fractions of all the element types \mathcal{A} existing in the structures, i.e., $\kappa \equiv \mathcal{A}$. Therefore, in the definition (1) of $\mathbf{f}^{(0)}$, $n_{\kappa \equiv \mathcal{A}}^{(0)}$ is the number of atoms of element \mathcal{A} . This fingerprint is a three-dimensional vector whose components satisfy a simple normalization condition $\sum_{\mathcal{A} \in \{\text{C, O, H}\}} f_{\mathcal{A}}^{(i)} = 1$.

B. First-order fingerprint $\mathbf{f}^{(1)}$

Next in the hierarchy is the case $\kappa \equiv \mathcal{A}i$, in which $n_{\kappa \equiv \mathcal{A}i}^{(1)}$ is the number of \mathcal{A} atoms which are i -fold coordinated. $\mathbf{f}^{(1)}$ is a six-dimensional vector satisfying several constraints established from the definition or from the chemistry. The first one is the normalization condition, given as

$$\sum_{\mathcal{A}i} f_{\mathcal{A}i}^{(1)} = 1. \quad (2)$$

Within the two data sets, all the C2 atoms should be grouped by pairs, forming triple $\text{C} \equiv \text{C}$ bonds. Therefore, the number of C2 atoms, which is $N_{at} f_{\text{C}2}^{(1)}$, must be an even integer. Moreover, since each C3 atom makes only a double bond with either an O1 atom or another C3 atom, one must have $f_{\text{C}3}^{(1)} \geq f_{\text{O}1}^{(1)}$

while $N_{\text{at}}[f_{\text{C3}}^{(1)} - f_{\text{O1}}^{(1)}]$ is an even number. By examining the connectivity of a structure, another constraint reads

$$f_{\text{H1}}^{(1)} - 2f_{\text{C4}}^{(1)} - f_{\text{C3}}^{(1)} + f_{\text{O1}}^{(1)} = \frac{2}{N_{\text{at}}}(1 - N_{\text{O}} - d), \quad (3)$$

where N_{O} is the number of closed loops of bonds and d is a structure-dependent parameter. For molecules and crystals composed of isolated substructures (or molecules), $d = 0$, while for crystals composed of connected substructures, $d > 0$. The derivation of this constraint is given in Appendix A. The last constraint of $\mathbf{f}^{(1)}$ is written in the form of a recursion relation, i.e.,

$$\sum_i f_{\text{Ai}}^{(1)} = f_{\text{A}}^{(0)}. \quad (4)$$

C. Second-order fingerprint $\mathbf{f}^{(2)}$

Both $\mathbf{f}^{(0)}$ and $\mathbf{f}^{(1)}$ are local, representing the density of the atom types of a material. The equilibrium interatomic distance is somehow captured by the second-order fingerprint $\mathbf{f}^{(2)}$ where all the possible bonds are counted. $\mathbf{f}^{(2)}$ is a 13-dimensional vector whose components $f_{\text{Ai-Bj}}^{(2)}$ represent the normalized number $n_{\text{Ai-Bj}}^{(2)}$ of the Ai-Bj bonds in the structure. From $\mathbf{f}^{(2)}$, $\mathbf{f}^{(1)}$ can readily be determined by a recursion relation

$$f_{\text{Ai}}^{(1)} = \sum_{\text{Bj}} \frac{2^{\delta_{\text{Ai,Bj}}-1}}{i} f_{\text{Ai-Bj}}^{(2)}, \quad (5)$$

where $\delta_{\text{Ai,Bj}}$ is used to remove the double counting when $\text{Ai} \equiv \text{Bj}$ [see Appendix B for the derivation of (5)]. Through this recursion relation, all the constraints that $\mathbf{f}^{(1)}$ obeys are applicable for $\mathbf{f}^{(2)}$. We note that $\mathbf{f}^{(2)}$ was discussed in several previous works, e.g., in Refs. [25,46,47] under the name of “bond counting.” This fingerprint can also be regarded as a generalization of “doubles,” the fingerprint defined in Ref. [20] for the chain models of polymers.

D. Third-order fingerprint $\mathbf{f}^{(3)}$

In the third-order fingerprint $\mathbf{f}^{(3)}$, the number of two-bond catenation is represented, i.e., $\kappa \equiv \text{Ai-Bj-Ck}$. In particular, the definition (1) for $f_{\kappa \equiv \text{Ai-Bj-Ck}}^{(3)}$ involves $n_{\text{Ai-Bj-Ck}}$, which is the number of Ai-Bj-Ck sequences, or, equivalently, the catenation of two bonds Ai-Bj and Bj-Ck . Considering compounds of C, O, and H, there are 125 possible distinct catenations of two bonds Ai-Bj and Bj-Ck . From $\mathbf{f}^{(3)}$, $\mathbf{f}^{(2)}$ can be determined as (see Appendix B)

$$\begin{aligned} f_{\text{Ai-Bj}}^{(2)} &= \sum_{\text{Ck}} \left[\frac{2^{\delta_{\text{Ai,Ck}}-1}}{j-1} f_{\text{Ai-Bj-Ck}}^{(3)} \right] \\ &= \sum_{\text{Ck}} \left[\frac{2^{\delta_{\text{Bj,Ck}}-1}}{i-1} f_{\text{Bj-Ai-Ck}}^{(3)} \right]. \end{aligned} \quad (6)$$

Similar to $\mathbf{f}^{(2)}$, $\mathbf{f}^{(3)}$ can be viewed as a generalization of “triples,” the fingerprint examined in Ref. [20].

IV. PROPERTY PREDICTION MODEL

A learning model is critical in order to map the fingerprints to properties. In this work, we chose Gaussian kernel

ridge regression (KRR) [5,48,49], the technique which has successfully been used in material properties predictions [20,25,28–30]. Within this model, the input fingerprints are transformed into higher-dimensional space whereby a linear relation between the transformed fingerprints and the associated properties can be established. This mapping involves the distances between fingerprints and can be regarded as a similarity-based prediction model; that is, similar properties may be predicted for materials with similar fingerprints.

In the KRR model, the property \mathcal{P}_{μ} of a structure μ is predicted as a weighted sum of Gaussians,

$$\mathcal{P}_{\mu} = \sum_{\nu} \alpha_{\nu} \exp \left[-\frac{1}{2} \left(\frac{d_{\mu\nu}}{\sigma} \right)^2 \right], \quad (7)$$

where ν runs over all the fingerprints in the training data set. Here, $d_{\mu\nu}$ is the distance between fingerprints μ and ν , defined as the Euclidean metric $d_{\mu\nu} = \sqrt{\sum_{\kappa} (f_{\kappa}^{\mu} - f_{\kappa}^{\nu})^2}$. The Gaussian width parameter σ and the regression coefficients α_{ν} are determined within the training phase when a regularized objective function is minimized [5,48,49]. During this phase, σ and the regularization parameter are determined by k -fold cross validation on the training set ($k = 5$ in this work). Within this method, the training data set is split into k bins; any of the bins is considered to be a new test data set, while the remaining

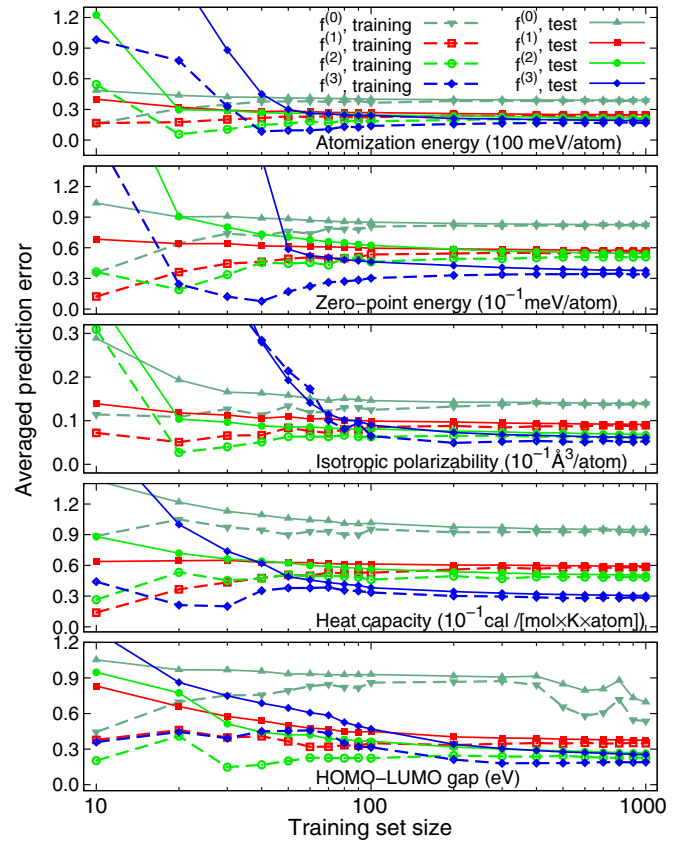


FIG. 2. (Color online) Learning curves corresponding to \mathcal{E}_{at} , \mathcal{E}_{ZP} , α , C_v , and E_{HL} . For each model, $\mathbf{f}^{(0)}$, $\mathbf{f}^{(1)}$, $\mathbf{f}^{(2)}$, and $\mathbf{f}^{(3)}$ are used to represent the molecules. Calculated data are given by symbols, while curves are a guide for the eye.

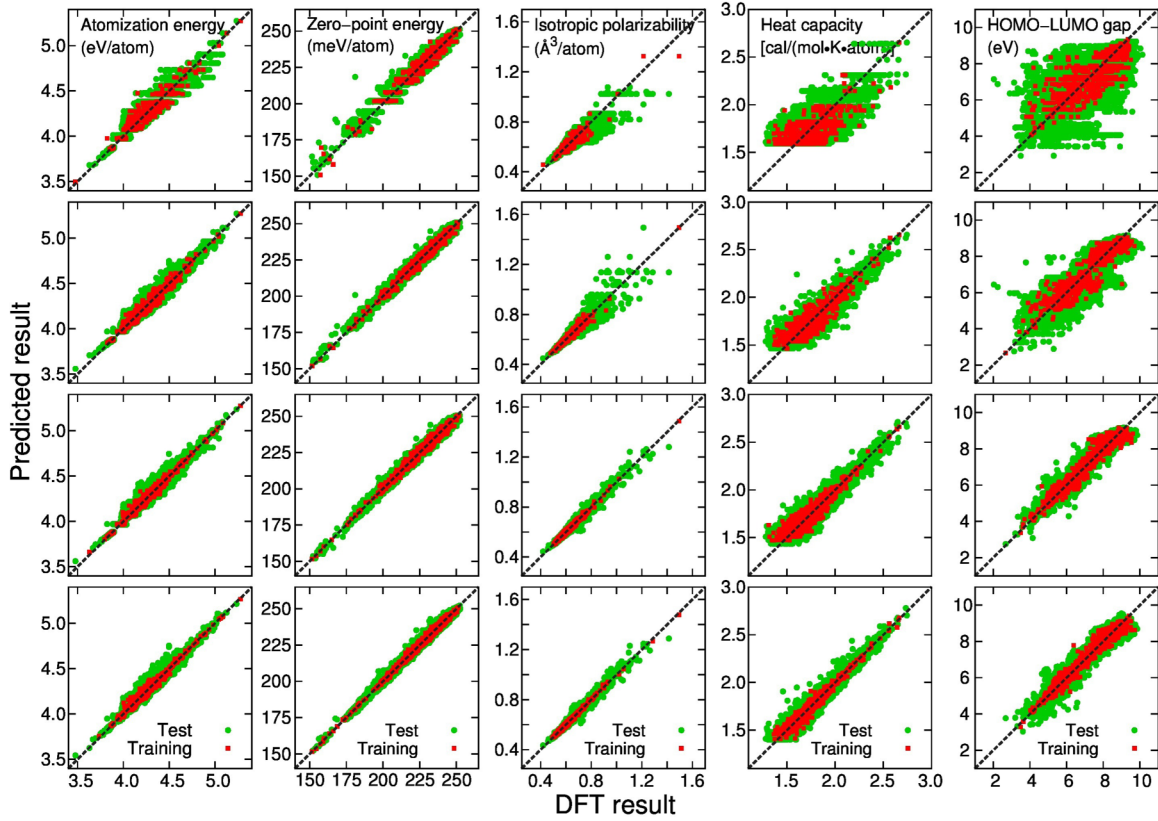


FIG. 3. (Color online) Predictions for \mathcal{E}_{at} , \mathcal{E}_{ZP} , α , C_v , and E_{HL} of the molecule data set, using $\mathbf{f}^{(0)}$, $\mathbf{f}^{(1)}$, $\mathbf{f}^{(2)}$, and $\mathbf{f}^{(3)}$ (from top row to bottom row). For each prediction, the training data set consists of 1000 points, while the test data set includes the remaining 44 708 data points.

$k - 1$ bins form a new training data set. This procedure is repeated for each of the k bins and for every value of σ and λ on a preselected logarithmic-scale grid. The optimal values of σ and λ , i.e., those leading to the minimum k -fold cross-validation (mean absolute) error, are used to compute α_v of the entire data set.

V. PROPERTY PREDICTION RESULTS

A. Molecule data set

The four fingerprints considered, namely, $\mathbf{f}^{(0)}$, $\mathbf{f}^{(1)}$, $\mathbf{f}^{(2)}$, and $\mathbf{f}^{(3)}$, were used to represent the molecule data set. To mimic the learning and prediction processes, the data set was randomly partitioned into a training data set and a test data set. The KRR model was then trained on the training data set using fivefold cross validation before predictions were made on the test data set. We show in Fig. 2 the learning curves of \mathcal{E}_{at} , \mathcal{E}_{ZP} , α , C_v , and E_{HL} , plotting the training and test errors against the number of molecules in the training data set (data reported in Fig. 2 were averaged over 30 independent runs). In addition, predictions for the test data set of 44 708 molecules after training the KRR model on a data set of 1000 molecules are shown in Fig. 3. As discussed in detail below, both Figs. 2 and 3 indicate that all of these properties can be very well predicted by using either $\mathbf{f}^{(2)}$ or $\mathbf{f}^{(3)}$, provided that the KRR model is trained on a training data set of $\simeq 200$ or more data points.

The general tendency, as revealed by Fig. 2, is that higher-order fingerprints offer more accurate predictions. The

zeroth-order fingerprint $\mathbf{f}^{(0)}$ can be used to roughly estimate energy-related quantities, i.e., \mathcal{E}_{at} and \mathcal{E}_{ZP} , while it cannot be used for others. For instance, E_{HL} cannot be predicted with $\mathbf{f}^{(0)}$ because this fingerprint is totally local in nature, encoding no information at any finite range. Consequently, the finite conjugation length, known to signal the energy-gap reduction in complex (conjugated) systems (see, for example, Ref. [50]), is not captured by $\mathbf{f}^{(0)}$. Fingerprints of higher orders, e.g., $\mathbf{f}^{(1)}$, $\mathbf{f}^{(2)}$, and $\mathbf{f}^{(3)}$, contain some information at increasing ranges, allowing for systematically better predicting E_{HL} . These fingerprints also work sufficiently well in predicting \mathcal{E}_{at} and \mathcal{E}_{ZP} . With $\mathbf{f}^{(1)}$, the average error in predicting \mathcal{E}_{at} is $\simeq 25$ meV/atom, while this error is reduced to $\simeq 20$ meV/atom and $\simeq 18$ meV/atom if $\mathbf{f}^{(2)}$ and $\mathbf{f}^{(3)}$, respectively, are used. The very good power of $\mathbf{f}^{(2)}$ in predicting \mathcal{E}_{at} reproduces the similar conclusions drawn for the bond-counting fingerprint by Ref. [47]. This behavior is understandable because the dissociation energy of chemical bonds in organic molecules and crystals, which dominates the stability of these systems, is well defined [46] in the same fashion as the bond length, as previously discussed. Interestingly, this predictive power can significantly be improved if more advanced fingerprints, i.e., those that can capture the small perturbations of interatomic distances like the Coulomb matrix, are used [29,30]. Compared to $\mathbf{f}^{(1)}$ and $\mathbf{f}^{(2)}$, $\mathbf{f}^{(3)}$ is significantly better in predicting C_v . The considerable improvement in the predictions of α when $\mathbf{f}^{(2)}$ is used instead of $\mathbf{f}^{(1)}$ may indicate the key contribution from polar bonds to the high-value regime of α .

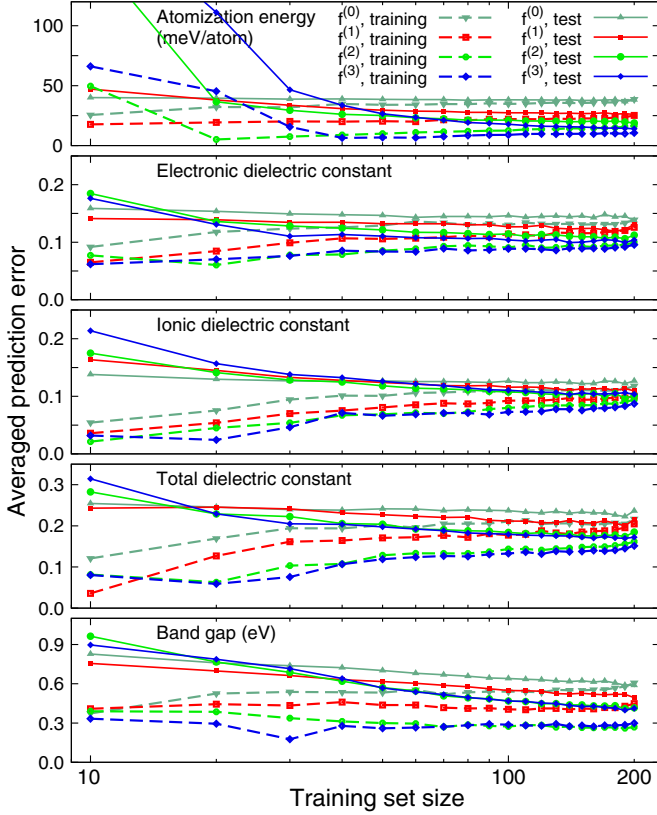


FIG. 4. (Color online) Learning curves corresponding to \mathcal{E}_{at} , ϵ_{elec} , ϵ_{ion} , ϵ , and E_g determined by using $\mathbf{f}^{(0)}$, $\mathbf{f}^{(1)}$, $\mathbf{f}^{(2)}$, and $\mathbf{f}^{(3)}$ for representing the crystals structures. Calculated data are shown by symbols, while curves are a guide for the eye.

B. Crystal data set

We performed similar predictions for the data set of 215 crystals containing C, O, and H. Using the KRR model coupled with $\mathbf{f}^{(0)}$, $\mathbf{f}^{(1)}$, $\mathbf{f}^{(2)}$, and $\mathbf{f}^{(3)}$, five properties of these crystals, including the atomization energies \mathcal{E}_{at} , the band gap E_g , the electronic dielectric constant ϵ_{elec} , the ionic dielectric constant ϵ_{ion} , and the total dielectric constant $\epsilon_{\text{tot}} = \epsilon_{\text{elec}} + \epsilon_{\text{ion}}$, were predicted. We show in Fig. 4 the learning curves, representing the errors of the predictions using these fingerprints, averaged over 100 independent runs. In Fig. 5, the predictions for the five properties are given using the KRR model trained on a random training set of 150 data points.

Clearly, the tendency of the prediction performances on the crystal data set is similar to that of the molecule data set; that is, high accuracies are obtained with fingerprints of higher orders, and properties which are governed by long-range information, e.g., band gap E_g , can be predicted with only high-order fingerprints. For the atomization energy \mathcal{E}_{at} , predictions with $\mathbf{f}^{(0)}$ and $\mathbf{f}^{(1)}$ lead to quite high average errors, which reduced to $\simeq 18$ and $\simeq 15$ meV/atom when $\mathbf{f}^{(2)}$ and $\mathbf{f}^{(3)}$, respectively, were used. Overall, all five examined properties can be predicted well when high-order fingerprints are used to represent the crystals. For instance, by employing $\mathbf{f}^{(3)}$, the average error in predicting E_g is $\simeq 0.45$ eV, while the electronic dielectric constant ϵ_{elec} and the ionic dielectric constant ϵ_{ion} can be predicted with an average error of 0.1–0.2.

VI. UTILITIES OF THE FINGERPRINTS

The demonstrated predictive power of the KRR model, which uses $\mathbf{f}^{(i)}$ to represent materials structures, inspires the idea of using this model to rationally optimize materials for a targeted property \mathcal{P}_{opt} , a concept often referred to as “inverse design” [51–54]. In fact, a large number of success stories along this direction have been reported in the past, using various approaches, e.g., iteratively optimizing the properties of a given compound or *on-the-fly* screening when searching for stable structures [9,55–66]. Here, our idea is that starting from a trained KRR model, fingerprints which correspond to the desired properties can be predicted. Then, molecular structures will be reconstructed from the predicted fingerprints. Finally, the targeted properties will be verified by DFT calculations at the same level as those used for the training data set.

The greatest challenge of this procedure is to ensure that the predicted fingerprint is physically and chemically meaningful; that is, at least one material structure can be reconstructed from it [67,68]. Therefore, one must mathematically define the subspace of the meaningful fingerprints and then limit the search for desired fingerprints within this subspace. We present two approaches which can be used for designing molecules (the work of designing crystals is not considered here).

A. Design via enumeration

The central idea of this approach is that the components of a given fingerprint can be enumerated in a given way so that it is meaningful. We used $\mathbf{f}^{(2)}$ for a demonstration because predictions using this fingerprint are good, while its dimensionality is not too high like that of $\mathbf{f}^{(3)}$. We first implemented the applicable rules involving bonds and coordination numbers by defining five “backbone” blocks. They include C4, C = C (a pair of C3 atoms with a double bond), C \equiv C (a pair of C2 atoms with a triple bond), C = O (one C3 and one O1 atom linked by a double bond), and O2. By definition, all of the dangling bonds starting from these blocks are single bonds; thus any of them can be connected to others without any constraint. Then, given a set of backbone blocks, all the possible arrangements can be scanned, keeping track of the connectivity to eliminate some dangling bonds and saturating the remaining dangling bonds by either H1 or OH, referred to as “ending” blocks. From the obtained arrangements, $\mathbf{f}^{(2)}$ could be unambiguously determined, and their properties were predicted. Those with targeted properties were singled out to rebuild molecular structures for validating calculations. We show in Fig. 6 two optimized molecules constructed from two of the predicted fingerprints, labeled by A and B, accompanied by the predicted and calculated E_{HL} and α . The results given in Fig. 6 indicate that the desired molecules are indeed obtained.

B. Design via inversion

Different from the enumeration approach, this procedure aims to directly determine the fingerprints, starting from

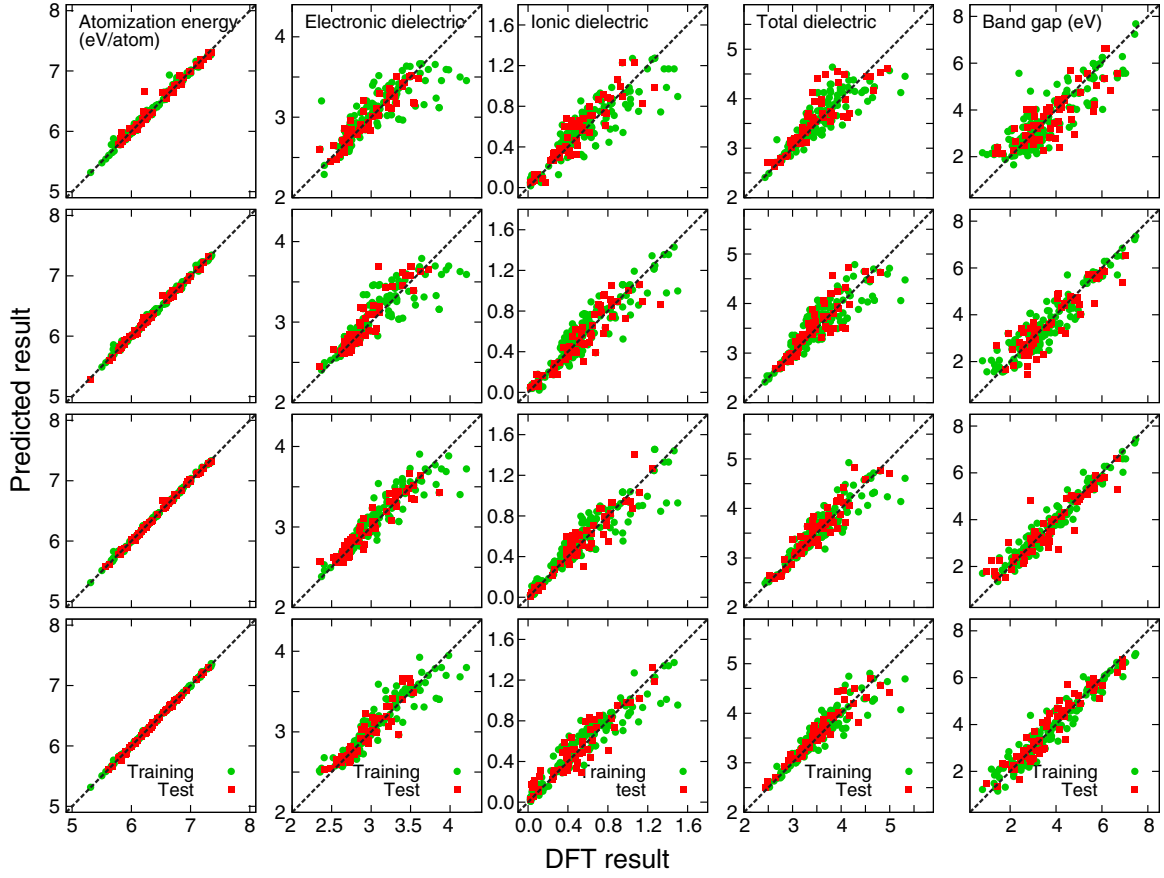


FIG. 5. (Color online) Predictions for \mathcal{E}_{at} , ϵ_{elec} , ϵ_{ion} , ϵ , and E_{gap} of the crystal data set, using $\mathbf{f}^{(0)}$, $\mathbf{f}^{(1)}$, $\mathbf{f}^{(2)}$, and $\mathbf{f}^{(3)}$ (from top row to bottom row). For each prediction, the training set size is 150, and the remaining 70 points form the test set.

desired properties. This goal can be achieved by optimizing an objective function, aiming towards the desired properties while applying the constraints that ensure the fingerprints considered are meaningful. Because the reconstruction step requires a simple enough fingerprint, $\mathbf{f}^{(1)}$ was selected for this approach. Among the constraints established for $\mathbf{f}^{(1)}$, (2) and (3) are

explicitly imposed in the objective function

$$G[\mathbf{f}^{(1)}, \lambda_1, \lambda_2] = (\mathcal{P} - \mathcal{P}_{\text{opt}})^2 + \lambda_1 \left[\sum_{Ai} f_{Ai}^{(1)} - 1 \right]^2 + \lambda_2 [f_{H1}^{(1)} - 2f_{C4}^{(1)} - f_{C3}^{(1)} + f_{O1}^{(1)}]^2. \quad (8)$$

Here, λ_1 and λ_2 are the Lagrange multipliers associated with the constraints, while \mathcal{P} is the property (or properties) of the trial fingerprint $\mathbf{f}^{(1)}$ predicted by the trained KRR model. In practice, we evaluated \mathcal{P} by averaging many predictions; each of them was given by the KRR model trained on a randomly selected training data set of 1000 data points. All the terms in (8) are given in the quadratic form to smoothen G . Generally, the problem of minimizing $G[\mathbf{f}^{(1)}, \lambda_1, \lambda_2]$ (performed with simulated annealing [69] in this work) returns many solutions $\mathbf{F}^{(1)}$. For each of them, N_{at} was determined by minimizing another objective function $D[\mathbf{F}]$, defined as

$$D[\mathbf{F}^{(1)}] = \sum_{Ai} [N_{\text{at}} F_{Ai}^{(1)} - \text{nint}(N_{\text{at}} F_{Ai}^{(1)})]^2, \quad (9)$$

where $\text{nint}(x)$ returns the closest integer to x . Once N_{at} is determined, a postscreening step is performed to consider the

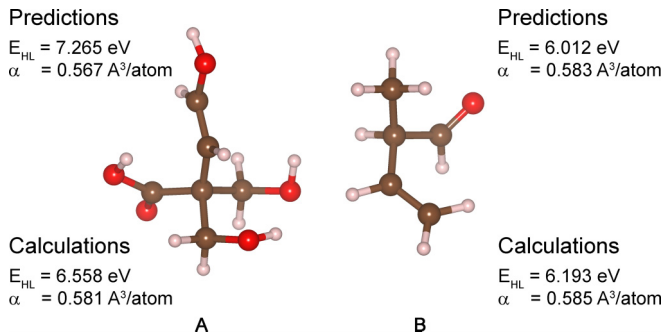


FIG. 6. (Color online) Optimized molecules, constructed from two predicted fingerprints A and B, shown with the predicted and calculated values of E_{HL} and α . Carbon, oxygen, and hydrogen atoms are given in dark brown, red, and pink, respectively.

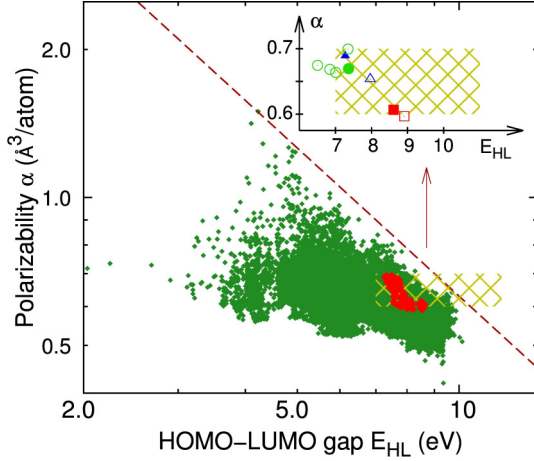


FIG. 7. (Color online) $E_{\text{HL}} - \alpha$ log-log plot of the molecule data set, shown by green symbols, with the predicted fingerprints shown by red diamonds within the regime of desired properties, i.e., $0.6 \leq \alpha \leq 0.7 \text{ \AA}^3/\text{atom}$ and $E_{\text{HL}} \geq 7.0 \text{ eV}$. In the inset, the predicted and calculated properties of the molecules reconstructed from three predicted fingerprints, i.e., C, D, and E, are shown by solid and open symbols: triangles for C, circles for D, and squares for E. The dashed line sketches the limit $\alpha \sim 1/E_{\text{HL}}$ addressed in the text.

possibility of $N_{\text{O}} > 0$ and to single out the fingerprints so that $N_{\text{at}}F_{\text{C2}}^{(1)}$ and $N_{\text{at}}[F_{\text{C3}}^{(1)} - F_{\text{O1}}^{(1)}]$ are positive even numbers. Such fingerprints are meaningful; that is, molecules can be built up from any of them.

We demonstrate this procedure by optimizing two properties simultaneously, i.e., the HOMO-LUMO gap E_{HL} and the isotropic polarizability α . Because α is a measure of the response, in terms of charge redistribution, of a molecule to the external electric field, this quantity is closely related to the electronic contribution of the dielectric constant ϵ_{elec} . We note that these properties seem to be competing, as shown in Fig. 7, where an asymptotic limit of the form $\alpha \sim 1/E_{\text{HL}}$ can be seen (a similar limit between two related properties of crystals, namely, ϵ_{elec} and E_{g} , was documented earlier in Ref. [70]). An examination of Fig. 3 reveals that the prediction of α using $\mathbf{f}^{(1)}$ is fairly good in the region of $\alpha < 0.8 \text{ \AA}^3/\text{atom}$. For this reason, we searched for new molecules, i.e., those that do not exist in the molecule data set, for which $0.6 \leq \alpha \leq 0.7 \text{ \AA}^3/\text{atom}$ while $E_{\text{HL}} \geq 7 \text{ eV}$ and show the results in Fig. 7. While the calculated E_{HL} of the molecule data set can reach the upper limit of $\simeq 10 \text{ eV}$, all the predictions for E_{HL} by the KRR model are below 9 eV . The reason is given in Fig. 3, which clearly implies that when $\mathbf{f}^{(1)}$ is coupled with the KRR model, high values of E_{HL} ($8 \leq E_{\text{HL}} \leq 10 \text{ eV}$) are generally underestimated by roughly 1 eV . Three of the predicted fingerprints, labeled by C, D, and E, were selected for rebuilding new molecules. From either C or E, only one molecule can be constructed, while many different molecules correspond to D. All of the molecules reconstructed from C, D, and E were optimized, and then their α and E_{HL} were calculated with GAUSSIAN 09 [71], using the 6-31G(2df,p) basis set and the B3LYP XC functional [72,73]. The results are summarized in Table I and in the inset of Fig. 7, demonstrating that the molecules with desired values of α and E_{HL} were actually obtained. Detailed

TABLE I. Predicted and calculated values of α (in $\text{\AA}^3/\text{atom}$) and E_{HL} (in eV) of the molecules designed from three predicted fingerprints, C, D, and E. Data from this table are also shown in the inset of Fig. 7.

Label	N_{at}	Predicted		Calculated	
		α	E_{HL}	α	E_{HL}
C	11	0.689	7.273	0.654	7.964
D	18	0.670	7.363	0.664–0.699	6.502–7.348
E	14	0.607	8.612	0.597	8.909

information on all of the designed molecules can be found in the Supplemental Material [42].

C. Remarks

It is worth noting that the key feature of $\mathbf{f}^{(i)}$ which is usable for the described enumeration and inversion design procedures is their discontinuity with respect to slight configurational perturbations. Because all the possible chemical bonds appearing in a molecule comprising C, O, and H are well defined, it is very likely that the optimization step performed on the reconstructed molecules preserves the predicted fingerprint. Moreover, the efficiency of the design approaches depends on several factors, including the prediction accuracy of the fingerprints used. Although predictions using high-order fingerprints are systematically better, the complexity generated by their high dimensionality is significant. Compared to the procedure described above, that utilizing $\mathbf{f}^{(2)}$ or $\mathbf{f}^{(3)}$ needs roughly 10 or 100 more constraints to ensure the considered fingerprints are meaningful. If the dimensionality of $\mathbf{f}^{(2)}$ can be considerably reduced, it may then be used for the inversion approach.

VII. CONCLUSIONS

To summarize, we have systematically studied a family of motif-based topological fingerprints which can numerically represent major classes of molecules and crystals. By using a similarity-based learning algorithm, these fingerprints can be mapped onto various properties of molecules and crystals, thus leading to an accelerated property prediction capability. A major advantage of these fingerprints is clearly demonstrated via two procedures for designing molecules, one by enumeration and the other by inversion. These procedures rely on the accelerated property prediction capability to identify the desired fingerprints and then to reconstruct molecules that possess one or more targeted properties. We note that although only molecules and crystals comprising C, O, and H are considered in this contribution, our results can straightforwardly be generalized to those containing other light elements whose coordination preferences are well established, e.g., N and F.

ACKNOWLEDGMENTS

The authors thank V. Botu, G. Pilania, and V. Sharma for useful discussions and O. Anatole von Lilienfeld for drawing our attention to some important relevant works. The present

work was supported by Multidisciplinary University Research Initiative (MURI) grant from the Office of Naval Research under Award No. N00014-10-1-0944. Computational work was made possible through XSEDE computational resource allocation number TG-DMR080058N [74].

APPENDIX A: CONSTRAINT ON $f^{(1)}$ DERIVED FROM ELEMENTARY CHEMICAL RULES

Constraint (3) was derived with an assumption that the desired molecular structure is connected; that is, any pair of atoms is connected by at least one sequence of the allowed chemical bonds. Let us take a molecule in which n_{Ai} is the number of blocks Ai . Starting from the applicable chemical rules, all the twofold-coordinated carbon atoms are grouped by pairs, forming $n_{C2}/2$ units of $C \equiv C$, each of which is a pair of carbon atoms linked by a triple bond. Next, n_{O1} onefold-coordinated oxygen atoms must bond with n_{O1} threefold-coordinated carbon atoms to form n_{O1} units of $C = O$. Then, the remaining $n_{C3} - n_{O1}$ threefold-coordinated carbon atoms are grouped together by pairs, forming $(n_{C3} - n_{O1})/2$ units of $C = C$. Therefore, the set of blocks Ai now contains $n_{C2}/2 + n_{O1} + (n_{C3} - n_{O1})/2 + n_{C4} + n_{O2}$ units of $C \equiv C$, CO , $C = C$, $C4$, and $O2$. Assuming that these units are isolated, the total number of dangling bonds starting from them is $2(n_{C2}/2) + 2n_{O1} + 4[(n_{C3} - n_{O1})/2] + 4n_{C4} + 2n_{O2}$, or simply

$$n_{C2} + 2n_{C3} + 4n_{C4} + 2n_{O2}. \quad (A1)$$

By joining $n_{C2}/2 + n_{O1} + (n_{C3} - n_{O1})/2 + n_{C4} + n_{O2}$ units together, the number of dangling bonds that will be annihilated to form interunit bonds is $2[n_{C2}/2 + n_{O1} + (n_{C3} - n_{O1})/2 + n_{C4} + n_{O2} - 1] + 2n_{O1}$, where n_{O1} is the number of loops of bonds, each of which costs two extra bonds. Therefore, the number of remaining dangling bonds is

$$n_{C3} + 2n_{C4} - n_{O1} - 2n_{O1} + 2. \quad (A2)$$

All of these dangling bonds must be saturated by n_{H1} hydrogen atoms; thus,

$$n_{H1} = n_{C3} + 2n_{C4} - n_{O1} - 2n_{O1} + 2. \quad (A3)$$

The constraint (3) can then be obtained when we divide Eq. (A3) by N_{at} . This constraint is applicable not only for molecules but also for crystals formed by repeatedly placing an isolated molecule in a periodic grid. If these molecules are not isolated, i.e., if they form a network of d dimensions,

$2d$ dangling bonds are used to form the network (assuming that the network is formed by only single bonds). Thus, Eq. (A3) is given as

$$n_{H1} = n_{C3} + 2n_{C4} - n_{O1} - 2n_{O1} - 2d + 2. \quad (A4)$$

In the general case when not only single bonds are involved in the network formation, the parameter d used in Eq. (A4) is not necessarily an integer.

APPENDIX B: DERIVATION OF THE RECURSION RELATIONS OF $f^{(2)}$ AND $f^{(3)}$

1. Recursion relations of $f^{(2)}$

The number n_{Ai} of blocks Ai can be determined by counting all the bonds of the $Ai-Bj$ type. By summing all the number of $Ai-Bj$ bonds, the $Ai-Ai$ bonds are counted twice. Therefore,

$$n_{Ai} = \frac{1}{i} \left[\sum_{Bj} n_{Ai-Bj} - \frac{1}{2} n_{Ai-Ai} \right]. \quad (B1)$$

Then, the recursion relation of $f^{(2)}$ can be obtained by dividing (B1) by the total number of atoms N_{at} .

2. Recursion relations of $f^{(3)}$

Similar to the derivation of (B1), the fingerprint component $f_{Ai-Bj}^{(2)}$ can be determined by counting the number of $Ai-Bj-Ck$ sequences before dividing by $j - 1$. In such a procedure, the $Ai-Bj-Ai$ sequences are counted twice. Thus, after removing the double counting, we obtain

$$n_{Ai-Bj} = \frac{1}{j-1} \left[\sum_{Ck} n_{Ai-Bj-Ck} - \frac{1}{2} n_{Ai-Bj-Ai} \right]. \quad (B2)$$

We note that one can also count the number of $Bj-Ai-Ck$ sequences before dividing the total number by $i - 1$. Thus,

$$n_{Ai-Bj} = \frac{1}{i-1} \left[\sum_{Ck} n_{Bj-Ai-Ck} - \frac{1}{2} n_{Bj-Ai-Bj} \right]. \quad (B3)$$

By dividing (B2) and (B3) by N_{at} , two equivalent recursion relations are obtained. Moreover, we note that (B2) and (B3) set up a constraint that $f^{(3)}$ must also satisfy.

- [1] G. Hautier, A. Jain, and S. Ong, *J. Mater. Sci.* **47**, 7317 (2012).
- [2] S. Curtarolo, G. L. W. Hart, M. B. Nardelli, N. Mingo, S. Sanvito, and O. Levy, *Nat. Mater.* **12**, 191 (2013).
- [3] V. Sharma, C. C. Wang, R. G. Lorenzini, R. Ma, Q. Zhu, D. W. Sinkovits, G. Pilania, A. R. Oganov, S. Kumar, G. A. Sotzing, S. A. Boggs, and R. Ramprasad, *Nat. Commun.* **5**, 4845 (2014).
- [4] T. Mueller, A. G. Kusne, and R. Ramprasad, in *Reviews in Computational Chemistry*, edited by A. L. Parrill and K. B. Lipkowitz (Wiley, New York, 2016).

- [5] T. Hastie, R. Tibshirani, and J. Friedman, *The Elements of Statistical Learning: Data Mining, Inference, and Prediction*, 2nd ed. (Springer, New York, 2009).
- [6] C. M. Breneman and M. Rhem, *J. Comput. Chem.* **18**, 182 (1997).
- [7] N. Sukumar, M. Krein, Q. Luo, and C. Breneman, *J. Mater. Sci.* **47**, 7703 (2012).
- [8] T. Le, V. C. Epa, F. R. Burden, and D. A. Winkler, *Chem. Rev.* **112**, 2889 (2012).

- [9] S. Curtarolo, D. Morgan, K. Persson, J. Rodgers, and G. Ceder, *Phys. Rev. Lett.* **91**, 135503 (2003).
- [10] K. Rajan, *Mater. Today* **8**, 38 (2005).
- [11] J. C. Schön, *Z. Anorg. Allg. Chem.* **640**, 2717 (2014).
- [12] B. Meredig, A. Agrawal, S. Kirklin, J. E. Saal, J. W. Doak, A. Thompson, K. Zhang, A. Choudhary, and C. Wolverton, *Phys. Rev. B* **89**, 094104 (2014).
- [13] K. Hansen, G. Montavon, F. Biegler, S. Fazli, M. Rupp, M. Scheffler, O. A. von Lilienfeld, A. Tkatchenko, and K.-R. Müller, *J. Chem. Theor. Comput.* **9**, 3404 (2013).
- [14] R. Guha and A. Bender, *Computational Approaches in Cheminformatics and Bioinformatics* (Wiley, New York, 2011).
- [15] A. Varnek, in *Cheminformatics and Computational Chemical Biology*, edited by J. Bajorath, Methods in Molecular Biology Vol. 672 (Humana, New York, 2011), pp. 213–243.
- [16] A. Jain, S. P. Ong, G. Hautier, W. Chen, W. D. Richards, S. Dacek, S. Cholia, D. Gunter, D. Skinner, G. Ceder, and K. A. Persson, *APL Mater.* **1**, 011002 (2013).
- [17] G. Bergerhoff, I. Brown, F. Allen, G. Bergerhoff, and R. Sievers, *Crystallographic Databases* (International Union of Crystallography, Chester, 1987).
- [18] S. Gražulis, A. Daškevič, A. Merkys, D. Chateigner, L. Lutterotti, M. Quirós, N. R. Serebryanaya, P. Moeck, R. T. Downs, and A. Le Bail, *Nucleic Acids Res.* **40**, D420 (2012).
- [19] R. Ramakrishnan, P. O. Dral, M. Rupp, and O. A. von Lilienfeld, *Sci. Data* **1**, 140022 (2014).
- [20] G. Pilania, C. Wang, X. Jiang, S. Rajasekaran, and R. Ramprasad, *Sci. Rep.* **3**, 2810 (2013).
- [21] A. N. Andriotis, G. Mpourmpakis, S. Broderick, K. Rajan, S. Datta, M. Sunkara, and M. Menon, *J. Chem. Phys.* **140**, 094705 (2014).
- [22] H. C. Dam, T. L. Pham, T. B. Ho, A. T. Nguyen, and V. C. Nguyen, *J. Chem. Phys.* **140**, 044101 (2014).
- [23] R. D. Brown and Y. C. Martin, *J. Chem. Inf. Comput. Sci.* **36**, 572 (1996).
- [24] R. D. Brown and Y. C. Martin, *J. Chem. Inf. Comput. Sci.* **37**, 1 (1997).
- [25] M. Rupp, A. Tkatchenko, K.-R. Müller, and O. A. von Lilienfeld, *Phys. Rev. Lett.* **108**, 058301 (2012).
- [26] K. Hansen, F. Biegler, O. A. von Lilienfeld, K.-R. Müller, and A. Tkatchenko (unpublished).
- [27] O. A. von Lilienfeld, R. Ramakrishnan, M. Rupp, and A. Knoll, *Int. J. Quantum Chem.* **115**, 1084 (2015).
- [28] V. Botu and R. Ramprasad, *Int. J. Quantum Chem.* **115**, 1074 (2015).
- [29] R. Ramakrishnan, P. O. Dral, M. Rupp, and O. A. von Lilienfeld, *J. Chem. Theory Comput.* **11**, 2087 (2015).
- [30] R. Ramakrishnan and O. A. von Lilienfeld, *Chimia* **69**, 182 (2015).
- [31] S. Goedecker, in *Modern Methods of Crystal Structure Prediction*, edited by A. R. Oganov (Wiley-VCH, Weinheim, Germany, 2011), Chap. 7, pp. 147–180.
- [32] S. Goedecker, *J. Chem. Phys.* **120**, 9911 (2004).
- [33] M. Amsler and S. Goedecker, *J. Chem. Phys.* **133**, 224104 (2010).
- [34] C. W. Glass, A. R. Oganov, and N. Hansen, *Comput. Phys. Commun.* **175**, 713 (2006).
- [35] G. Kresse and J. Hafner, *Phys. Rev. B* **47**, 558 (1993).
- [36] G. Kresse, Ph.D. thesis, Technische Universität Wien, 1993.
- [37] G. Kresse and J. Furthmüller, *J. Comput. Mater. Sci.* **6**, 15 (1996).
- [38] G. Kresse and J. Furthmüller, *Phys. Rev. B* **54**, 11169 (1996).
- [39] E. D. Murray, K. Lee, and D. C. Langreth, *J. Chem. Theor. Comput.* **5**, 2754 (2009).
- [40] H. J. Monkhorst and J. D. Pack, *Phys. Rev. B* **13**, 5188 (1976).
- [41] K. Lee, É. D. Murray, L. Kong, B. I. Lundqvist, and D. C. Langreth, *Phys. Rev. B* **82**, 081101(R) (2010).
- [42] See Supplemental Material at <http://link.aps.org/supplemental/10.1103/PhysRevB.92.014106> for more than 200 structural files relevant to this paper in POSCAR or xyz format.
- [43] L. Pauling, *J. Am. Chem. Soc.* **54**, 3570 (1932).
- [44] F. H. Allen, O. Kennard, D. G. Watson, L. Brammer, A. G. Orpen, and R. Taylor, *J. Chem. Soc., Perkin Trans. 2*, S1 (1987).
- [45] F. H. Allen, D. G. Watson, L. Brammer, A. G. Orpen, and R. Taylor, in *International Tables for Crystallography, Mathematical, Physical and Chemical Tables*, 3rd ed., edited by E. Prince (Kluwer Academic, Norwell, MA, 2004), Chap. 9.5.
- [46] S. W. Benson, *J. Chem. Educ.* **42**, 502 (1965).
- [47] J. E. Moussa, *Phys. Rev. Lett.* **109**, 059801 (2012).
- [48] T. Hofmann, B. Schölkopf, and A. J. Smola, *Ann. Stat.* **36**, 1171 (2008).
- [49] K. Muller, S. Mika, G. Ratsch, K. Tsuda, and B. Schölkopf, *IEEE Trans. Neural Networks* **12**, 181 (2001).
- [50] P. Stallinga, *Electrical Characterization of Organic Electronic Materials and Devices* (Wiley, Chester, UK, 2009).
- [51] G. Ceder, Y. M. Chiang, D. R. Sadoway, M. K. Aydinol, Y. I. Jang, and B. Huang, *Nature (London)* **392**, 694 (1998).
- [52] F. Besenbacher, I. Chorkendorff, B. S. Clausen, B. Hammer, A. M. Molenbroek, J. K. Nørskov, and I. Stensgaard, *Science* **279**, 1913 (1998).
- [53] A. Franceschetti and A. Zunger, *Nature (London)* **402**, 60 (1999).
- [54] T. Weymuth and M. Reiher, *Int. J. Quantum Chem.* **114**, 823 (2014).
- [55] O. A. von Lilienfeld, R. D. Lins, and U. Rothlisberger, *Phys. Rev. Lett.* **95**, 153002 (2005).
- [56] V. Marcon, O. A. von Lilienfeld, and D. Andrienko, *J. Chem. Phys.* **127**, 064305 (2007).
- [57] O. A. von Lilienfeld, *J. Chem. Phys.* **131**, 164102 (2009).
- [58] D. Sheppard, G. Henkelman, and O. A. von Lilienfeld, *J. Chem. Phys.* **133**, 084104 (2010).
- [59] M. Wang, X. Hu, D. N. Beratan, and W. Yang, *J. Am. Chem. Soc.* **128**, 3228 (2006).
- [60] S. Keinan, X. Hu, D. N. Beratan, and W. Yang, *J. Phys. Chem. A* **111**, 176 (2007).
- [61] S. Keinan, W. D. Paquette, J. J. Skoko, D. N. Beratan, W. Yang, S. Shinde, P. A. Johnston, J. S. Lazo, and P. Wipf, *Org. Biomol. Chem.* **6**, 3256 (2008).
- [62] B. C. Rinderspacher, J. Andzelm, A. Rawlett, J. Dougherty, D. N. Beratan, and W. Yang, *J. Chem. Theor. Comput.* **5**, 3321 (2009).
- [63] J. Greeley and M. Mavrikakis, *Nat. Mater.* **3**, 810 (2004).
- [64] M. d’Avezac, J.-W. Luo, T. Chanier, and A. Zunger, *Phys. Rev. Lett.* **108**, 027401 (2012).
- [65] H. J. Xiang, B. Huang, E. Kan, S.-H. Wei, and X. G. Gong, *Phys. Rev. Lett.* **110**, 118702 (2013).

- [66] C. L. Phillips and G. A. Voth, [Soft Matter](#) **9**, 8552 (2013).
- [67] O. A. von Lilienfeld, [Int. J. Quantum Chem.](#) **113**, 1676 (2013).
- [68] O. A. von Lilienfeld and M. E. Tuckerman, [J. Chem. Phys.](#) **125**, 154104 (2006).
- [69] S. Kirkpatrick, C. D. Gelatt, and M. P. Vecchi, [Science](#) **220**, 671 (1983).
- [70] C. C. Wang, G. Pilania, S. A. Boggs, S. Kumar, C. Breneman, and R. Ramprasad, [Polymer](#) **55**, 979 (2014).
- [71] M. J. Frisch *et al.*, GAUSSIAN 09, revision A.02, Gaussian, Inc., Wallingford, CT, 2009.
- [72] A. D. Becke, [J. Chem. Phys.](#) **98**, 5648 (1993).
- [73] P. J. Stephens, F. J. Devlin, C. F. Chabalowski, and M. J. Frisch, [J. Phys. Chem.](#) **98**, 11623 (1994).
- [74] J. Towns, T. Cockerill, M. Dahan, I. Foster, K. Gaither, A. Grimshaw, V. Hazlewood, S. Lathrop, D. Lifka, G. D. Peterson, R. Roskies, J. R. Scott, and N. Wilkins-Diehr, [Comput. Sci. Eng.](#) **16**, 62 (2014).